Molecular and Cellular Biochemistry Faculty Publications | Molecular and Cellular Biochemistry

7-2017

Mutations in the Transmembrane Domain and Cytoplasmic Tail of Hendra Virus Fusion Protein Disrupt Virus-Like-Particle Assembly

Nicolás P. Cifuentes-Muñoz
University of Kentucky, ncifuentes@uky.edu

Weina Sun
The Pennsylvania State University

Greeshma Ray
The Pennsylvania State University

Phuong Tieu Schmitt
The Pennsylvania State University

Stacy Webb
University of Kentucky, stacy.webb@uky.edu

See next page for additional authors

Repository Citation

Authors
Nicolás P. Cifuentes-Muñoz, Weina Sun, Greeshma Ray, Phuong Tieu Schmitt, Stacy Webb, Kathleen Gibson, Rebecca Ellis Dutch, and Anthony P. Schmitt

Mutations in the Transmembrane Domain and Cytoplasmic Tail of Hendra Virus Fusion Protein Disrupt Virus-Like-Particle Assembly

Mutations in the Transmembrane Domain and Cytoplasmic Tail of Hendra Virus Fusion Protein Disrupt Virus-Like-Particle Assembly

Nicolás Cifuentes-Muñoz,[a] Weina Sun,[b] Greeshma Ray,[b] Phuong Tieu Schmitt,[b] Stacy Webb,[a] Kathleen Gibson,[a] Rebecca Ellis Dutch,[a] Anthony P. Schmitt[b]

Department of Molecular and Cellular Biochemistry, University of Kentucky College of Medicine, Lexington, Kentucky, USA[a]; Department of Veterinary and Biomedical Sciences, The Pennsylvania State University, University Park, Pennsylvania, USA[b]

ABSTRACT Hendra virus (HeV) is a zoonotic paramyxovirus that causes deadly illness in horses and humans. An intriguing feature of HeV is the utilization of endosomal protease for activation of the viral fusion protein (F). Here we investigated how endosomal F trafficking affects HeV assembly. We found that the HeV matrix (M) and F proteins each induced particle release when they were expressed alone but that their coexpression led to coordinated assembly of virus-like particles (VLPs) that were morphologically and physically distinct from M-only or F-only VLPs. Mutations to the F protein transmembrane domain or cytoplasmic tail that disrupted endocytic trafficking led to failure of F to function with M for VLP assembly. Wild-type F functioned normally for VLP assembly even when its cleavage was prevented with a cathepsin inhibitor, indicating that it is endocytic F trafficking that is important for VLP assembly, not proteolytic F cleavage. Under specific conditions of reduced M expression, we found that M could no longer induce significant VLP release but retained the ability to be incorporated as a passenger into F-driven VLPs, provided that the F protein was competent for endocytic trafficking. The F and M proteins were both found to traffic through Rab11-positive recycling endosomes (REs), suggesting a model in which F and M trafficking pathways converge at REs, enabling these proteins to preassemble before arriving at plasma membrane budding sites.

IMPORTANCE Hendra virus and Nipah virus are zoonotic paramyxoviruses that cause lethal infections in humans. Unlike that for most paramyxoviruses, activation of the henipavirus fusion protein occurs in recycling endosomal compartments. In this study, we demonstrate that the unique endocytic trafficking pathway of Hendra virus F protein is required for proper viral assembly and particle release. These results advance our basic understanding of the henipavirus assembly process and provide a novel model for the interplay between glycoprotein trafficking and paramyxovirus assembly.

KEYWORDS Hendra, endocytic trafficking, fusion, matrix, Rab11, virus assembly

The Hendra (HeV), Nipah (NiV), and Cedar viruses are members of the *Henipavirus* genus within the *Paramyxoviridae* family (1). These zoonotic viruses can cause severe illness in both animals and humans, with reported mortality rates of up to 90% (2). The natural reservoirs of henipaviruses are bats of the Pteropodidae family, and transmissions to other species, including pigs, horses, and humans, have resulted in multiple recent spillovers (2–4). The geographic expansion of these bat species, the wide host ranges of these viruses, and the recent findings of seropositive bats in African countries raise concern about future spillovers of henipaviruses (5). The lack of thera-

peutic and preventive strategies against these pathogens has led to their classification as category C agents restricted to biosafety level 4 (BSL4) facilities (6).

Henipavirus virions are enveloped pleomorphic particles which can range in size from 40 nm to 1,900 nm (7, 8). The ribonucleoprotein (RNP) complex, located within the virion, is composed of the single-stranded negative-sense RNA genome coated by the N protein at a ratio of one N protein to six nucleotides (9). The phosphoprotein (P) and the large RNA-dependent RNA polymerase (L) are also bound to RNPs and are necessary for transcription and replication of the genome. Underlying the viral envelope is the matrix protein (M), which has a major role in assembly of particles and determination of viral architecture. Paramyxovirus M proteins fulfill a "bridge" role, interacting at the same time with the inner viral components (10, 11) and with the cytoplasmic tails (CTs) of viral envelope glycoproteins (12, 13). The virion surface is densely packed with two protruding transmembrane (TM) glycoproteins: the attachment protein (G), involved in receptor recognition, and the fusion protein (F), which has a major role in the membrane fusion required for viral entry. Although much progress has been made in understanding the entry of henipaviruses, their assembly and exit from cells are less well understood.

Unlike those of other paramyxoviruses, an intriguing feature of the henipavirus life cycle is the utilization of the endosomal protease cathepsin L for proteolytic activation of the viral fusion protein (14, 15). Henipavirus F is a 546-amino-acid type I integral membrane protein that contains different domains, including a fusion peptide (FP), two heptad repeat regions (HRA and HRB), a TM domain, and the cytoplasmic tail. After synthesis in the endoplasmic reticulum (ER), the F protein is transported through the secretory pathway to the plasma membrane as an uncleaved precursor form termed F_0. This protein is then endocytosed through Rab5-positive early endosomes and cleaved by cathepsin L in early and recycling endosomal compartments to generate the disulfide-linked heterodimer F_1+F_2 (14–18). In cell lines with reduced cathepsin L levels, NiV F cleavage can alternatively be performed by cathepsin B in early endosomal compartments (19). Following cathepsin cleavage, the F_1+F_2 heterodimer is recycled back to the plasma membrane through Rab4-positive recycling endosomes (REs), where it is incorporated into nascent virions (18). An important endocytosis motif, YSRL, is present in the cytoplasmic tails of henipavirus F proteins, and mutations targeting this motif affect endocytic recycling (20–22). In addition, mutations of residues S490 and Y498, located in the TM domain of F, affect endocytic recycling and trafficking (18). Interestingly, the henipavirus attachment glycoprotein G, a type II integral membrane protein, undergoes secretory pathway trafficking at a lower rate than that of the F protein, and it has been postulated that physical interactions between G and F do not occur in the ER but rather at later times, most likely at viral assembly sites (23, 24). As virions of henipaviruses are composed of a mixture of uncleaved and cleaved F proteins (16), it remains to be elucidated what consequences the F recycling pathway has with respect to the trafficking and assembly of other viral components, including G and M.

To coordinate virus assembly, paramyxovirus M proteins must ultimately coalesce with other viral components at selected sites on infected cell plasma membranes from which viral budding will occur. The specific route that an M protein takes within a cell to arrive at this destination likely plays a key role in its functionality. For example, M proteins of henipaviruses and other paramyxoviruses transit through the nucleus at early times postinfection (25, 26) and interact with several nuclear and nucleolar host factors, such as fibrillarin (26, 27). M protein mutants that fail to traffic through the nucleus cannot function in particle budding (25). Interaction with the endosomal pathway may also be important for the function of the paramyxovirus M protein in many cases. Henipavirus M proteins can bind to AP-3 adapter complexes that function to allow trafficking of proteins between endosomal compartments (28). Viral RNPs (vRNPs) of influenza virus and several paramyxoviruses traffic through Rab11-positive REs, allowing efficient, polarized delivery of viral genomes to virus assembly sites (29–33). The Rab11 effector, Rab11-FIP2, is required for the late stages of respiratory
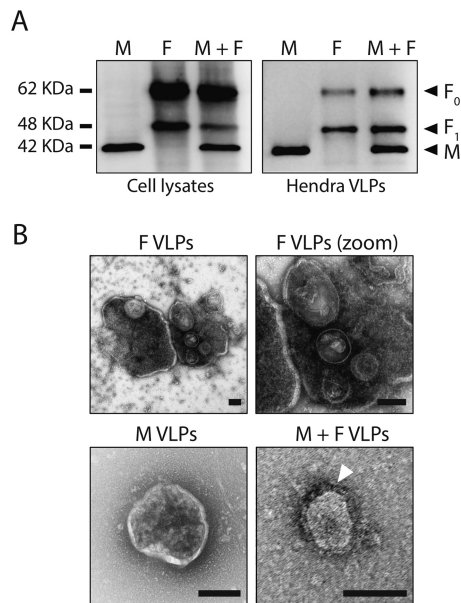
FIG 1 HeV M protein aids in proper assembly of F into VLPs. (A) 293T cells were transfected to produce the HeV M and F proteins either separately or together. Viral proteins from cell lysates and from purified VLP fractions were detected by immunoblotting. (B) 293T cells were transfected to produce the HeV F and M proteins either separately or together. VLPs were purified by centrifugation through sucrose cushions, adsorbed to carbon-coated grids, and visualized by transmission electron microscopy after negative staining. The white arrowhead indicates the spike layer present on M+F VLPs. Bars = 100 nm.

syncytial virus budding from polarized epithelial cells, allowing cell exit to occur in an ESCRT-independent manner (34).

In the present work, we investigated the potential impacts of henipavirus F protein endocytic trafficking and cathepsin cleavage on virus assembly. We found that endocytic trafficking of HeV F is important for its assembly with M and for the formation of virus-like particles (VLPs), while cathepsin cleavage of F is dispensable for VLP assembly. We also obtained evidence suggesting that the HeV F and M protein trafficking pathways intersect at Rab11a-positive REs. Our findings support a model in which coordination between M and F proteins during virus assembly is achieved at least in part through the convergence of these proteins at RE compartments.

RESULTS

HeV M protein aids in proper assembly of F into VLPs. The minimal protein requirements necessary to assemble virus-like particles for members of the *Paramyxo-viridae* are different depending on the pathogen. While in some cases the M protein alone can assemble in the form of VLPs, this is not true for other paramyxoviruses, such as parainfluenza virus 5 (PIV5) and mumps virus (MuV) (35, 36). For henipaviruses, expression of M, G, or F alone is sufficient to assemble Nipah VLPs (28, 37, 38). We recently showed that M-only VLPs can also be produced for Hendra virus (28), but F, G, or the combination of those proteins for assembly of VLPs has not been examined for this virus. Thus, we initially analyzed the contributions of the M and F proteins, alone or together, to the assembly of Hendra VLPs. For this purpose, 293T cells were transfected with plasmids encoding F and M proteins either separately or together, and then the supernatants were collected and the purified particles analyzed by Western blotting. The F protein in the cell lysates was detected as two different bands, representing the uncleaved form F_0, of approximately 61 kDa, and the cleaved form F_1, of approximately 49 kDa, while the M protein was found at the expected size of 42 kDa (Fig. 1A). The F_2 protein was not visualized, as the antibodies used for Western blotting recognize an epitope in the F_1 subunit. Analysis of concentrated supernatants by Western blotting demonstrated that F and M, expressed individually or together, were
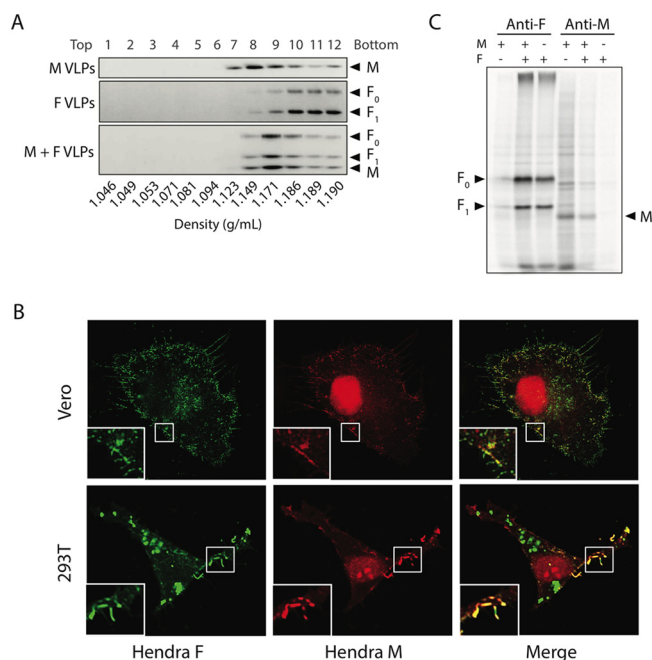
FIG 2 Coordination of HeV M and F proteins during VLP assembly. (A) 293T cells were transfected to produce the HeV F and M proteins either separately or together. VLPs were purified by centrifugation through sucrose cushions and then loaded onto the tops of 5% to 45% continuous sucrose gradients. After centrifugation, fractions were collected, and the viral proteins in each fraction were detected by immunoblotting. (B) Vero cells (upper panels) or 293T cells (lower panels) on glass coverslips were transfected to produce the HeV F and M proteins together. Cells were bound with an F-specific antibody, fixed, permeabilized, bound with an M-specific antibody, and then visualized by fluorescence microscopy. (C) 293T cells were transfected to produce the HeV F and M proteins either separately or together. Proteins synthesized in the transfected cells were metabolically labeled, cells were lysed, and immunoprecipitation was carried out using an anti-HeV F antibody or an anti-Myc-tag antibody (to detect the Myc-tagged M protein), as indicated. Proteins were detected using a phosphorimager.

released into supernatants, potentially in the form of VLPs (Fig. 1A). To determine if proteins detected in the supernatants of transfected cells were present in particles having a morphology consistent with VLPs, we performed electron microscopy (EM) studies using negative staining on F-only, M-only, and F+M purified supernatants. Interestingly, we rarely observed individual F-only VLPs but instead observed large vesicles of up to 1 μm in diameter, with spike-bearing putative virus-like particles enclosed within these vesicles (Fig. 1B, upper panels). These particles were observed in the supernatants of F-expressing cells but not mock-transfected cells. Some individual particles with spikes could sporadically be observed from the supernatants of F-expressing cells, but we cannot rule out the possibility that they resulted from the breakdown of large vesicles and leakage of their contents. M-only VLPs, on the other hand, were observed by EM as individual spikeless particles with sizes that typically ranged from 100 to 250 nm (average, 136 $\pm$ 46 nm). When supernatants of F+M-transfected cells were analyzed, smaller particles with protruding spikes (white arrowhead) that ranged in size from 50 to 150 nm (average, 83 $\pm$ 25 nm) were found (Fig. 1B). Furthermore, in the presence of M, the large vesicles containing smaller vesicles were no longer observed, suggesting an interplay between F and M during the budding of VLPs.

Coordination of HeV M and F proteins during VLP assembly. Although the HeV M and F proteins are each capable of inducing particle release from transfected cells, the above-described EM results suggest that M and F coexpression does not simply result in a mixture of M-only and F-only VLPs. To further investigate the nature of the VLPs produced upon M and F coexpression, M-only VLPs, F-only VLPs, and M+F VLPs were each analyzed by sucrose density gradient analysis (Fig. 2A). VLPs were loaded

onto the tops of 5% to 45% continuous sucrose gradients, and following ultracentrifugation, 12 fractions were collected and analyzed by immunoblotting. M-only VLPs were recovered primarily from fractions 7 to 10 of the gradient, with a peak in fraction 8, corresponding to a density of 1.149 g/ml. F-only VLPs, on the other hand, were found mainly in higher-density fractions 10 to 12 (1.186 to 1.190 g/ml). When M+F VLPs were analyzed, both the M and F proteins peaked together in fraction 9 of the gradient (1.171 g/ml), a result that is inconsistent with a VLP mixture composed of separate M-only and F-only particles. Instead, this result suggests that the M and F proteins assembled into a distinct population of particles with a density profile different from that of either M-only or F-only VLPs. This interpretation is in agreement with our EM observations showing that when both proteins were present, only spike-containing particles were found. Further evidence of coordination between M and F proteins was also obtained using fluorescence microscopy (Fig. 2B). For this purpose, Vero or 293T cells expressing the M and F proteins were bound with an F-specific antibody to visualize cell surface-localized F protein. Cells were then fixed and permeabilized prior to incubation with M-specific antibody. The M protein was found distributed throughout the cell cytoplasm, at the cell periphery, and in the cell nucleus, which is an intriguing feature of some paramyxovirus M proteins (25) (Fig. 2B). Bright spots potentially corresponding to accumulation of the protein in plasma membrane patches were observed (Fig. 2B, insets), and colocalization with cell surface-localized F protein was observed at these patches. In order to determine if colocalization was the result of a direct interaction between the M and F proteins, coimmunoprecipitation studies with cells expressing both proteins were performed. Cells were transfected, and 24 h later, proteins were radiolabeled using ^{35}S-containing medium. After the labeling period, cells were lysed, and the lysates were incubated with anti-M or anti-F antibody for immunoprecipitation. Neither F_0 nor F_1 was pulled down by using anti-Myc antibodies to immunoprecipitate Myc-M, nor was M pulled down by using anti-F serum for cells coexpressing both proteins (Fig. 2C). The same result was obtained by using a labeling time of 18 h to detect proteins made over a longer period or by immunoprecipitating the proteins directly from M+F VLPs (data not shown). These data suggest that the proteins do not stably interact in a way that is detectable using the immunoprecipitation procedures employed here. Overall, these results suggest that although both the HeV M and F proteins can induce particle release when expressed by themselves, the proteins likely coordinate with each other when coexpressed (not necessarily through a direct interaction), resulting in VLPs that contain both proteins.

Removal of the HeV F cytoplasmic tail impairs M+F VLP assembly. To assess the potential role of the cytoplasmic tail domain of F in VLP assembly and release, we constructed two deletion mutants of F with all or most of the CT domain removed (Fig. 3A). The putative transmembrane domain of HeV F spans residues V484 to K521, and the remaining 28 amino acid residues at the C-terminal end form the cytoplasmic tail. Both mutants, named ΔE519 and ΔG523 because they had deletions of the CT from residues 519 and 523, respectively, were first examined to determine the overall impacts of these mutations on protein function. Cell surface biotinylation of transfected Vero cells showed that both mutants reached the plasma membrane, mainly in the form of uncleaved protein (Fig. 3B). This result demonstrated that both proteins were trafficked through the secretory pathway and argued against potential misfolding due to the deletions. In line with this, cell-cell fusion assays showed that both mutant proteins could induce syncytium formation in Vero cells, indicating that these cytoplasmic tail-deleted proteins were functional. The levels of fusion were approximately 25% of the wild-type (wt) level, with smaller and less abundant syncytia observed (Fig. 3C), consistent with the low levels of cleavage for these mutant proteins. Next, the Hendra virus F deletion mutants were assessed for the ability to assemble in M+F VLPs. Total levels of F protein in cell lysates were not affected by the mutations, but a diffuse mixture of F_0 bands was detected for the ΔE519 and ΔG523 proteins, consistent with heterogeneous posttranslational modifications of these mutant proteins (Fig. 3D). The
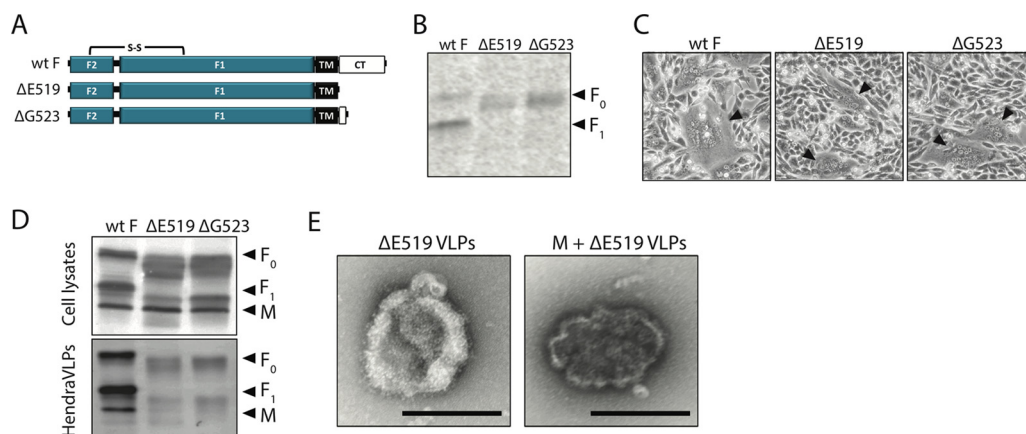
FIG 3 Removal of the HeV F cytoplasmic tail impairs VLP assembly. (A) Schematic illustration of the HeV F protein and its cytoplasmic tail truncations. (B) Vero cells were transfected to produce the indicated HeV F protein variants. Cells were metabolically labeled, surface proteins were biotinylated, cells were lysed, and immunoprecipitation was carried out using an anti-HeV F antibody. Proteins were detected using a phosphorimager. (C) Vero cells were transfected to produce the HeV F and G proteins, and syncytium formation (black arrowheads) was observed after 18 h posttransfection. (D) 293T cells were transfected to produce the HeV M protein together with the indicated HeV F protein variants. Viral proteins from cell lysates and from purified VLP fractions were detected by immunoblotting. (E) 293T cells were transfected to produce the F ΔE519 protein alone or the F ΔE519 protein together with the M protein, as indicated. VLPs were purified by centrifugation through sucrose cushions, adsorbed to carbon-coated grids, and visualized by transmission electron microscopy after negative staining. Bars = 100 nm.

ΔE519 and ΔG523 mutants were released into the supernatant at much lower efficiencies than that of wt M+F VLPs, and barely detectable levels of M protein were also observed. In addition, the uncleaved F_0 protein was primarily observed, likely because removing the CT interfered with F trafficking needed for cleavage by cathepsin L. EM analysis indicated that the small number of VLPs containing CT mutants exhibited a size similar to that of wt VLPs, with evident glycoprotein spikes (Fig. 3E). This was true regardless of whether M was coexpressed. These results suggest that removal of the cytoplasmic tail significantly affects the morphology and efficiency of budding structures when F is expressed alone, and also affects the efficiency of VLP formation when F is coexpressed with M.

Endocytic trafficking of HeV F protein is required for proper assembly with M. In contrast to other paramyxovirus F proteins, henipavirus F proteins reach the cell surface in the inactive, uncleaved form. The proteins are endocytosed from the plasma membrane, leading to their encounter with cathepsin proteases within early endosomes. Following cathepsin cleavage, the F protein is routed through recycling endosomes before returning to the plasma membrane for incorporation into budding virus particles. How this unique pathway benefits the virus is unclear. Based on the reductions in budding found for the ΔE519 and ΔG523 mutants, we hypothesized that the unique F protein activation pathway is required for coordination with the M protein during virus assembly. To test this, we first examined the HeV F S490A single point mutant. Our previous studies showed that this mutant F protein is endocytosis defective and is retained at the cell surface for extended periods, with little proteolytic cleavage (18). Here we examined the VLP production function of this mutant F protein (Fig. 4A). In contrast to wt F, the F S490A protein expressed alone induced little VLP release (data not shown), and coexpression of F S490A with M resulted in the production of M-VLPs that contained very little F protein (Fig. 4A). Hence, this F mutant had lost both its intrinsic VLP release function and its ability to assemble with M for VLP production. To rule out the possibility that it might be cathepsin L cleavage rather than endocytic trafficking that is important for F assembly function, VLP production experiments were performed in the presence of the general cysteine protease inhibitor E-64d. In agreement with previous findings, E-64d treatment blocked cleavage of the HeV F_0 precursor to the F_1+F_2 fusogenically active form (Fig. 4A, left panel). However, E-64d blockage of F protein cleavage did not impair incorporation of the wt F protein
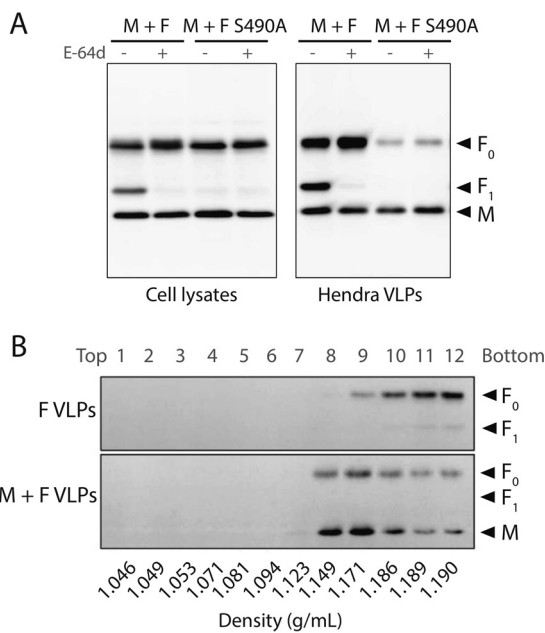
FIG 4 Endocytic trafficking of the HeV F protein is required for proper assembly with M. (A) 293T cells were transfected to produce the HeV M protein together with the HeV F protein or the HeV F S490A protein in the presence of the cathepsin inhibitor E-64d, as indicated. Viral proteins from cell lysates and from purified VLP fractions were detected by immunoblotting. (B) 293T cells were transfected to produce the HeV F protein alone or the HeV F protein together with the M protein, as indicated, in the presence of the cathepsin inhibitor E-64d. VLPs were purified by centrifugation through sucrose cushions and loaded onto the tops of 5% to 45% continuous sucrose gradients. After centrifugation, fractions were collected, and the viral proteins in each fraction were detected by immunoblotting.

into budding particles (Fig. 4A, right panel) and did not impair F-only VLP release (data not shown), demonstrating that proteolytic processing of F is not a prerequisite for its assembly functions. This is further demonstrated in Fig. 4B, which shows the results of F-VLPs and M+F VLPs from E-64d-treated cells being analyzed using sucrose density gradients. VLP-derived M and F proteins peaked in the same fractions even though E-64d treatment prevented proteolytic cleavage of F_0, indicating that cleavage of F was not required for F to assemble with M for VLP production. Together, these results suggest that proper assembly of F with M in preparation for VLP formation requires endocytic trafficking (but not proteolytic cleavage) of the F protein.

To further explore the relationship between F protein endocytic trafficking and virus particle assembly, we employed a series of F mutant proteins that in previous studies were found to exhibit defects at various stages of endocytosis and/or recycling (Fig. 5A and B). These mutant F proteins were coexpressed with the HeV M protein for VLP production, and F assembly function was quantified by calculating the ratio of the total F ($F_0 + F_1$) signal to the M signal (which remained nearly equal for each condition) in the VLP fraction (Fig. 5C and D). Two of the mutations, S490A and Y525A, are known to cause defects in F protein endocytosis, with the S490A mutation leading to a complete lack of endocytosis and the Y525A mutation leading to lower rates of endocytosis. Here we found that while the S490A mutation significantly impaired F-VLP assembly function, the Y525A mutation had no impact on F-VLP assembly. This suggests that while endocytic trafficking is necessary, even inefficient endocytosis of F is sufficient for the purpose of VLP assembly. Four additional mutations, S490V, S490E, S490K, and Y498A, did not impair F endocytosis but instead prevented the internalized protein from being efficiently recycled back to the cell surface. The S490V and Y498A mutants exhibited severe defects in recycling, and these mutations also led to significant reductions in VLP assembly function. The S490E and S490K mutants exhibited moderate defects in recycling, and these mutations led to only minor decreases in F assembly function. The S490T and Y498F mutations did not cause any defects in F
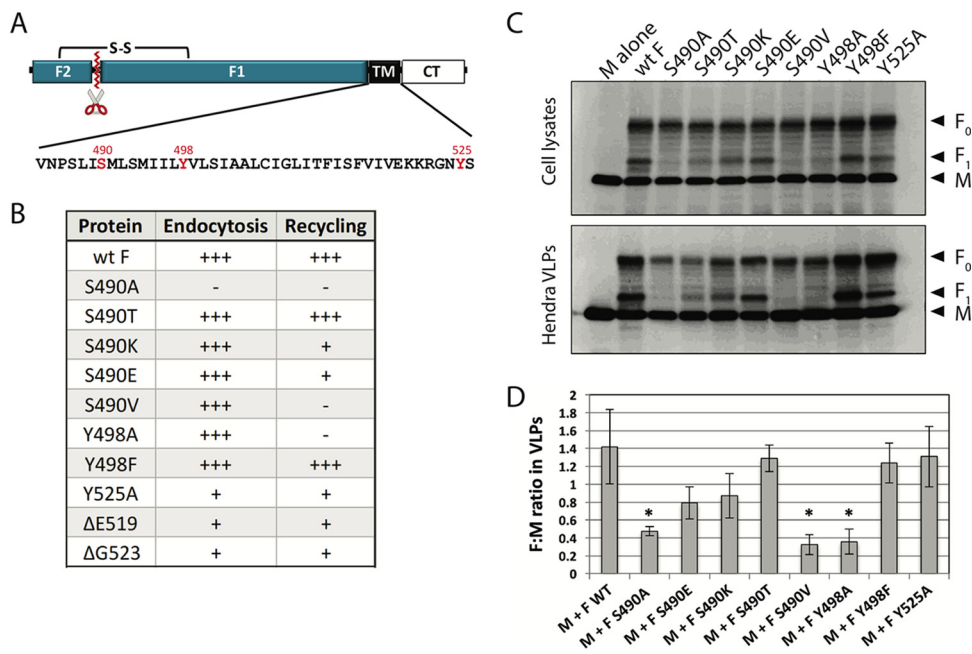
FIG 5 Severe defects to F protein endocytic trafficking correlate with poor VLP assembly. (A) Schematic illustrating the locations of HeV F protein mutations that affect its endocytic trafficking. (B) Table summarizing the defective phenotype of each F mutant relative to the wt phenotype. $+++$, wt level; $+$, less than 25% of WT level; $-$, not detectable. (C) 293T cells were transfected to produce the HeV M protein together with the indicated HeV F protein variants. Viral proteins from cell lysates and from purified VLP fractions were detected by immunoblotting. (D) The F:M ratios in the VLP fractions were calculated as follows: F:M ratio = (F_0 signal plus F_1 signal)/M signal. Error bars indicate standard deviations ($n = 3$). *, $P < 0.05$.

protein endocytosis or its subsequent recycling to the plasma membrane, and no VLP assembly defects were observed for these mutants. Overall, these results demonstrate that severe defects to either F protein endocytosis or F protein recycling correlate with poor VLP assembly function.

The VLP production experiments for Fig. 5 were performed under conditions of high-level M protein expression, and this led to abundant production of VLPs in all cases, with efficient incorporation of F protein into VLPs only when the F proteins were capable of undergoing endocytic trafficking. Paramyxovirus M proteins require a threshold level of protein expression for VLP or virion assembly, and severe defects in particle release are often observed if M protein expression is reduced (13, 39–42). Interestingly, we found that in cases where this threshold level of HeV M expression was not met, M incorporation into VLPs could still be rescued through coexpression of the HeV F protein (Fig. 6A). In this case, the amount of M plasmid used for transfection was reduced from 200 ng to 50 ng, leading to reduced (7-fold) M protein accumulation in the cell lysate fraction (data not shown). This resulted in very poor production of M-VLPs, but substantial rescue of M into the VLP fraction was observed upon F protein coexpression (Fig. 6A). Reduced M expression could also be accomplished by carrying out transfections using an alternative 293T cell line (referred to here as 293T-KY) that produces smaller quantities of M protein for any given amount of M plasmid used for transfection (cf. Fig. 6B and 5C). In this case, it is likely that the F protein provides most of the driving force for particle budding, with the M protein incorporated into the VLPs as a passenger. Using these conditions, we tested whether trafficking-altered F proteins could rescue M incorporation into VLPs. We found that the S490V and Y498A mutations caused severe defects and a near absence of any VLP production. The S490A, S490K, and S490E mutations caused moderate defects, and the S490T, Y498F, and Y525A mutations had no significant effect on VLP production. In all cases, the rescue of M incorporation into VLPs corresponded with the efficiency of F-VLP production (Fig. 6B and C), consistent with the idea that M is a passive participant in the budding process
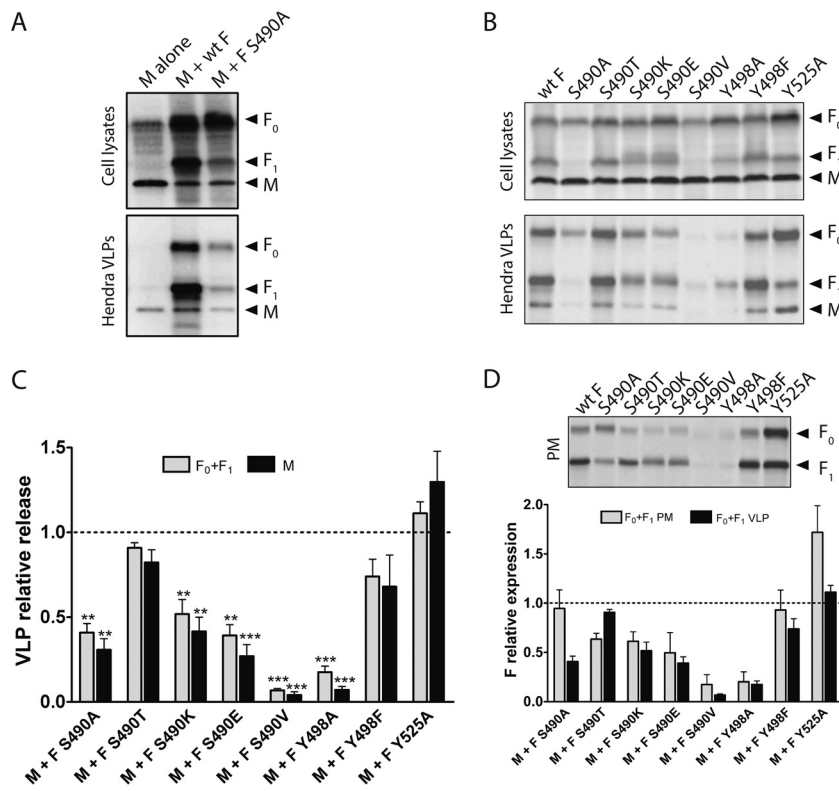
FIG 6 Severe defects in F protein endocytic trafficking correlate with poor VLP assembly under conditions of limiting M expression. (A) 293T-PSU cells were transfected to produce the HeV M protein together with the indicated HeV F protein variants. The M plasmid amount was reduced to 50 ng per dish (from the usual 200 ng per dish) to achieve conditions of limiting M expression. Viral proteins from cell lysates and from purified VLP fractions were detected by immunoblotting. (B) 293T-KY cells were transfected to produce the HeV M protein together with the indicated HeV F protein variants. Viral proteins from cell lysates and from purified VLP fractions were detected by immunoblotting. (C) The relative efficiency of VLP production was calculated either based on F protein content (as the amount of F_0 plus F_1 detected in VLPs divided by the amount detected in cell lysates, normalized to the value obtained with the wt F protein) or based on M protein content (as the amount of M detected in VLPs divided by the amount detected in cell lysates, normalized to the value obtained with the wt F protein) ($n = 6$). **, $P < 0.01$; ***, $P < 0.001$. (D) 293T-KY cells were transfected to produce the indicated HeV F protein variants. Surface-exposed proteins were biotinylated, cells were lysed, the biotinylated fraction was recovered, and the F protein was detected by immunoblotting. The amount of F signal was plotted, normalized to the value obtained with the wt F protein ($n = 3$). VLP production values obtained from panel C were plotted alongside the cell surface expression values.

under these conditions, able to be released only with the help of a budding-competent F protein. Interestingly, when cell surface expression of F protein variants was measured using a surface biotinylation assay, we found that the Y525A mutant exhibited enhanced cell surface expression compared to that of wt F (Fig. 6D). This did not lead to a corresponding increase in VLP production, however, as VLP release for this mutant was similar to that of wt F. Overall, the results obtained under conditions of limiting M expression paralleled those obtained with high-level M expression, with the exception of those for the S490A mutant, which displayed a less severe phenotype under M-limiting conditions.

Rab11 recycling endosomes play a role in HeV assembly. In an effort to explain why endocytic F trafficking is important for HeV particle assembly, we hypothesized that the M and F protein trafficking pathways might intersect one another at an intracellular compartment, facilitating assembly of the two proteins prior to their arrival at the cell surface for budding. To investigate this possibility, we examined M protein localization in transfected Vero cells compared to that of a series of marker proteins specific for the endoplasmic reticulum (E-cadherin), *trans*-Golgi apparatus (TGN46), *cis*-Golgi apparatus (GM130), late endosome/lysosome (LAMP-1), early endosome
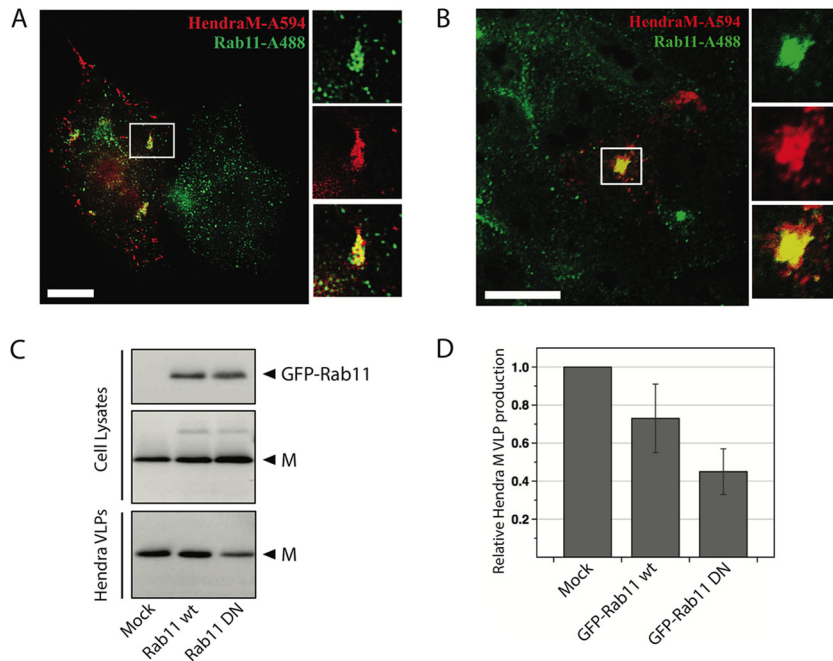
FIG 7 Rab11 recycling endosomes play a role in M-VLP assembly. Vero cells (A) or 293T cells (B) on glass coverslips were transfected to produce the HeV M protein, and subcellular localizations of M protein (red) and endogenous Rab11 (green) were visualized by immunofluorescence microscopy. (C) 293T cells were transfected to produce the HeV M protein together with GFP-Rab11 or dominant negative (DN) GFP-Rab11, as indicated. (D) The relative efficiency of VLP production was calculated as the amount of M detected in VLPs divided by the amount detected in cell lysates, normalized to the value obtained in the absence of Rab11 expression.

(EEA1), and recycling endosome (Rab11a). We observed colocalization between a portion of M protein and endogenous Rab11a (Fig. 7A) but not between M protein and any of the other markers (data not shown). The colocalization between M protein and Rab11a was also observed in transfected 293T cells (Fig. 7B). To assess the importance of Rab11 recycling endosomes for M budding function, M-only VLP production was measured in 293T cells transfected to produce dominant negative (DN) Rab11 (S25N). This resulted in a VLP production efficiency that was 2.2-fold reduced compared to normal levels (Fig. 7C and D).

The HeV F protein trafficking pathway is known to include the use of Rab5 and Rab4 endosomal compartments in order to achieve complete maturation of the protein and recycling to the plasma membrane (18), but potential localization of F to Rab11 compartments has not previously been examined. In transfected Vero cells as well as 293T cells, we observed a fraction of HeV F protein localized with endogenous Rab11a (Fig. 8A and B). In addition, we found that expression of dominant negative Rab11a reduced F-only VLP production by a factor of 4.4 (Fig. 8C and D). Together, these experiments define Rab11a-positive recycling endosome compartments as potential locations for coordinated assembly of F and M proteins prior to their arrival at the plasma membrane for particle budding.

DISCUSSION

In this study, we examined the interplay that occurs between the Hendra virus M and F proteins during their subcellular trafficking and subsequent assembly leading to particle release. Although we confirmed that both the HeV M and F proteins can induce particle release when expressed by themselves, we found that the M and F proteins coordinate with each other to form VLPs that are morphologically and physically distinct from either M-only or F-only VLPs. This coordination between the M and F proteins was apparent when we examined the wt F protein or F protein variants that retained the ability to undergo the normal F protein endocytic trafficking pathway.
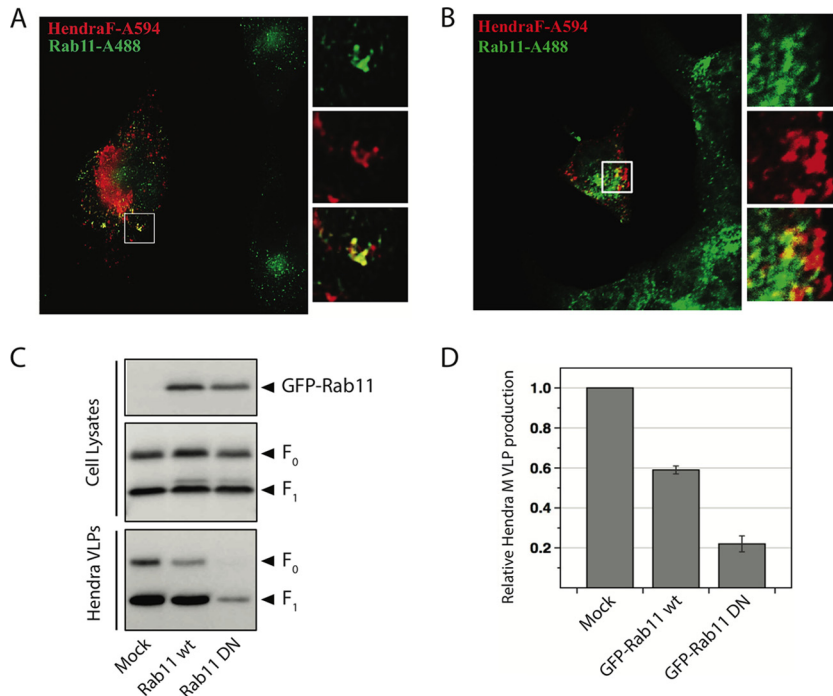
FIG 8 Rab11 recycling endosomes play a role in F-VLP assembly. Vero cells (A) or 293T cells (B) on glass coverslips were transfected to produce the HeV F protein, and subcellular localizations of F protein (red) and endogenous Rab11 (green) were visualized by immunofluorescence microscopy. (C) 293T cells were transfected to produce the HeV F protein together with GFP-Rab11 or dominant negative GFP-Rab11, as indicated. (D) The relative efficiency of VLP production was calculated as the amount of F_0 plus F_1 detected in VLPs divided by the amount detected in cell lysates, normalized to the value obtained in the absence of Rab11 expression.

However, mutant F proteins that failed to undergo endocytic trafficking and/or recycling back to the cell surface were assembly defective and did not coordinate with the M protein during VLP production, despite abundant accumulation of many of these mutant F proteins, such as F S490A, at the cell surface. Although these trafficking defects in many cases prevent proteolytic maturation of the F protein, as the protein cannot be cleaved unless it is endocytosed and trafficked to cathepsin-containing early endosome compartments, the proteolytic cleavage *per se* was not important for F protein assembly functions, as the wt F protein formed VLPs and was incorporated into M-VLPs even when its cleavage was prevented through treatment of cells with the cathepsin inhibitor E-64d. For this reason, we concluded that it is the endocytic trafficking of F protein, not its proteolytic cleavage, that is important for virus assembly. Evidence was obtained for the convergence of the F and M trafficking pathways at Rab11a-positive recycling endosomes, consistent with the possibility that the F and M proteins encounter one another on the membranes of recycling endosomes and then arrive at the plasma membrane preassembled and poised to induce particle budding.

The trafficking pathway of the henipavirus F glycoprotein is unique in the *Paramyxoviridae* family. After synthesis in the ER, the F glycoproteins of many paramyxoviruses, such as MuV, PIV5, human parainfluenza virus type 3 (HPIV3), and Newcastle disease virus (NDV), are processed by the ubiquitous subtilisin-like serine protease furin during transport through the *trans*-Golgi network, prior to arrival at the plasma membrane (43–46). For henipavirus F proteins, after trafficking through the secretory pathway to the plasma membrane, endocytic signals contained within the 28-residue F protein cytoplasmic tail as well as signals within the TM domain direct the protein to early endosomal compartments, where an encounter with cathepsin L proteases takes place to allow proteolytic maturation. The hydroxyl group of F protein TM domain residue S490 is critical for proper F protein endocytic trafficking, with an S490A mutation

causing failure of the protein to internalize from the cell surface and an S490V mutation causing failure of the internalized protein to recycle back to the cell surface (18). We found both of these trafficking-defective mutant F proteins to have an impaired virus assembly function, while the S490T variant, which retains its hydroxyl group and traffics similarly to the wt protein, exhibited no virus assembly defects. The aromatic ring of F TM domain residue Y498 is also critical for endocytic trafficking, with a Y498A mutation leading to F protein internalization but subsequent mistrafficking and failure to recycle to the cell surface (18). We found that the Y498A mutant F protein was defective for VLP assembly, while the Y498F protein was similar to the wt protein with respect to both endocytic trafficking and VLP assembly. The tyrosine-based motif ^{525}YSRL^{528} is important for F protein endocytosis, and mutation of residue Y525 alters internalization of the protein (20, 22). Recent work has also shown that mutation of residues Y525 and L528 results in a nonpolarized distribution of NiV F in neurons through disruption of the interaction with clathrin adaptor complex 1 (AP-1) components (47). The HeV F Y525A protein exhibited higher levels of cell surface expression than the wt F protein, leading to enhanced syncytium formation (Fig. 6D) (20). We found that the Y525A mutation did not lead to enhanced VLP assembly but rather led to an overall VLP production level that was similar to that of the wt F protein (and lower than wt VLP production levels if the results are normalized to cell surface expression levels). Overall, we found an almost complete correlation between F mutants with defects in endocytic trafficking and F mutants with virus assembly defects, consistent with a scenario in which proper assembly of F with M for VLP production is dependent on the endocytic recycling of F protein. This supports a previously undescribed role for the henipavirus F protein recycling pathway in viral assembly.

Rab11a is a member of the Rab11 small GTPase family that functions in regulating vesicular transport through endosome recycling (48). Rab11 proteins are involved in several cellular processes connected to intracellular vesicle trafficking, including protein secretion, protein targeting to tubular membrane structures, and apical membrane targeting in polarized cells. Interestingly, several negative-strand RNA viruses have been found to utilize Rab11-positive recycling endosomes during the trafficking of viral components in preparation for virion assembly. vRNPs of influenza virus, measles virus, and Sendai virus can all be found in Rab11-positive vesicles (29, 31, 49). Efficient polarized budding of respiratory syncytial virus is facilitated by Rab11a-enriched apical recycling endosomes (34, 50), and virus replication can be inhibited through expression of a dominant negative Rab11-FIP2 protein, leading to a late budding defect (34). Small interfering RNA (siRNA)-mediated depletion of Rab11 was found to negatively affect hantavirus release (51). We found for Hendra virus that both M-VLP and F-VLP production was impaired upon expression of a dominant negative Rab11 protein. Furthermore, the M protein and the F protein were each found partially localized to Rab11-positive recycling endosomes. These findings are consistent with a model in which the Hendra virus M protein and F protein trafficking pathways converge at recycling endosome compartments, providing an opportunity for viral components to concentrate and assemble prior to their final delivery to the cell surface for particle formation.

Matrix proteins of paramyxoviruses and other negative-strand RNA viruses are capable of directing particle assembly and release only after they have accumulated to a threshold level in cells (13, 39–42). This may potentially create an interesting dynamic for certain paramyxoviruses, including the henipaviruses, whose glycoproteins are independently capable of inducing particle release. Indeed, a matrixless Nipah virus was recovered by reverse genetics and is viable, albeit with severely defective infectivity and irregular particle morphology (52). Here we observed that the Hendra virus M protein, even expressed at a level below that required for budding function, could still assemble as a passenger in VLPs whose formation was driven by the F protein. Mutations that disabled endocytic F trafficking blocked F-driven particle release and thereby prevented the passenger M protein from exiting the cell (Fig. 6). This suggests that the threshold level of M protein needed to assemble with F might be lower than that needed for M to induce particle budding on its own. Such an arrangement may,

in theory, provide the virus with flexibility, allowing some infectious particles to be made even if protein accumulation within the infected cell has not reached optimal levels.

MATERIALS AND METHODS

Plasmids. cDNAs corresponding to HeV F and the F S490A, S490T, S490K, S490E, S490V, Y498A, Y498F, and Y525A mutants, all subcloned into pCAGGS vectors, have been described before (18, 20, 53). The HeV F cytoplasmic tail deletion mutants ΔE519 and ΔG523 were generated using the QuikChange site-directed mutagenesis system (Agilent Technologies, Santa Clara, CA), with the plasmid pGEM4Z-HeV F as the template. The constructs were verified by sequencing, and the F mutants were subcloned from pGEM into pCAGGS as previously described (20). cDNA corresponding to HeV M with an N-terminal Myc tag, subcloned into the pCAGGS vector, has been described before (28). The HeV M cDNA was also modified by PCR to replace the Myc tag with an N-terminal Flag tag, and this cDNA was subcloned into the expression vector pcDNATM3.1/myc-His(−)A (Thermo Fisher Scientific, Waltham, MA) for use in fluorescence microscopy experiments. Wild-type Rab11a and DN Rab11a S25N, cloned as N-terminal fusions with green fluorescent protein (GFP), were kind gifts from Gary Whittaker, Cornell University.

Cell lines. HEK 293T (PSU) cells were a kind gift of Robert Lamb, Northwestern University. HEK 293T (KY) cells were a kind gift of Judith White, University of Virginia. Vero cells were a kind gift of Biao He, University of Georgia. All cell lines were maintained in high-glucose Dulbecco's modified Eagle's medium (DMEM; Thermo Fisher Scientific) supplemented with 10% fetal bovine serum.

Measurements of VLP production. HEK 293T (KY) or HEK 293T (PSU) cells grown in 6-cm dishes to 70% to 80% confluence were transfected with pCAGGS plasmids encoding Myc-HeV M (0.2 μg/dish) and/or HeV F (1.0 μg/dish). Lipofectamine-Plus or Lipofectamine 2000 reagent (Thermo Fisher Scientific) in Opti-MEM was used for plasmid transfections. Total plasmid amounts were kept equal during transfection by using, when necessary, an empty pCAGGS plasmid that does not encode any protein. The VLP experiments for Fig. 1B, 2C, 3, and 6B to D were carried out using transfected HEK 293T (KY) cells, while the VLP experiments for Fig. 1A, 2A, 4, 5, 6A, 7, and 8 were carried out using transfected HEK 293T (PSU) cells. At 24 h posttransfection, the transfection medium was replaced with fresh growth medium. At 42 h posttransfection, cells and culture medium fractions were collected. The culture media were centrifuged at 8,000 × g for 2 min to remove cell debris. VLPs from the clarified culture medium fractions were then layered onto 20% sucrose cushions, and samples were centrifuged at 140,000 × g for 1.5 h, after which pellets containing VLPs were suspended in SDS-PAGE loading buffer containing 2.5% (wt/vol) dithiothreitol. For VLP production in the presence of a cathepsin inhibitor, E-64d (Sigma-Aldrich, St. Louis, MO) was added to both the transfection medium and the subsequent incubation medium, to a final concentration of 10 μM.

To prepare cell lysates, one-third of the cells from each sample were lysed with 0.1 ml of SDS-PAGE loading buffer. The lysates were centrifuged through QIAshredder homogenizers (Qiagen, Germantown, MD) to break up cell debris. Cell lysates and purified VLPs were fractionated by SDS-PAGE using 10% gels, and proteins were detected by immunoblotting using the anti-HeV F monoclonal antibody (MAb) 7C5 (a kind gift from Chris Broder, Uniformed Services University), the anti-Myc-tag monoclonal antibody 9E10 (Thermo Fisher Scientific) for detection of HeV M, or an anti-GFP polyclonal antibody (Clontech, Mountain View, CA) for detection of GFP-Rab11. Imaging and quantification were performed using either a LiCor Odyssey or Fuji FLA 7000 imaging system.

VLP density gradient analysis. HEK 293T (PSU) cells in 10-cm dishes were transfected with pCAGGS plasmids encoding Myc-HeV M (0.4 μg/dish), HeV F (1.6 μg/dish), or Myc-HeV M together with HeV F, and VLPs were isolated in the presence or absence of E-64d as described above. After centrifugation through 20% sucrose cushions, VLPs were resuspended in 200 μl of NTE buffer (0.1 M NaCl, 0.01 M Tris-HCl, pH 7.4, 0.001 M EDTA). VLPs were layered onto the tops of 5% to 45% continuous sucrose gradients prepared in NTE buffer. Gradients were centrifuged for 16 h at 150,000 × g, using a Sorvall AH650 swinging bucket rotor. Twelve fractions (0.3 ml [each]) were collected from top to bottom, and 15 μl of each fraction was resolved by SDS-PAGE using 10% gels. The HeV M and HeV F proteins were detected by immunoblotting as described above. Densities were calculated based on the measured weight and volume of each individual fraction.

Coimmunoprecipitation. HEK 293T (KY) cells grown in 6-cm dishes were transfected to produce the HeV F and/or M protein as described above. At 24 h posttransfection, cells were washed twice with 1× phosphate-buffered saline (PBS) and starved for 45 min in cysteine-methionine-deficient DMEM. Cells were labeled for 3 h by use of cysteine-methionine-deficient DMEM to which 35S was added (100 μCi/ml; MP Biomedicals, Irvine, CA). Following labeling, cells were washed twice with 1× PBS and then lysed with RIPA buffer (100 mM Tris-HCl [pH 7.4], 150 mM NaCl, 0.1% SDS, 1% Triton X-100, 1% deoxycholic acid containing 1:100 aprotinin [Calbiochem, San Diego, California], 1 mM phenylmethylsulfonyl fluoride [Sigma-Aldrich, St. Louis, MO], and 25 mM iodoacetamide [Sigma-Aldrich]). Following centrifugation at 136,500 × g for 10 min, the lysates were immunoprecipitated as previously described (54) with 10 μl of Hendra virus F protein-specific polyclonal serum or with 4 μl of anti-Myc monoclonal antibody 9E10. Samples were analyzed using 10% SDS-PAGE and visualized using a Typhoon FLA 7000 imager (GE Healthcare Life Sciences).

Cell surface biotinylation. To detect cell surface proteins by Western blotting, HEK 293T (KY) cells grown in 6-cm dishes were transfected as described above. At 48 h posttransfection, cells were biotinylated using a cell surface protein isolation kit (Thermo Fisher Scientific). The HeV F protein was then detected by immunoblotting using the biotinylated fraction, corresponding to plasma membrane

proteins. To detect cell surface proteins by immunoradiolabeling, Vero cells were transfected to produce the HeV F and/or M protein as described above. At 18 h posttransfection, cells were washed with PBS and starved for 45 min in DMEM deficient in cysteine and methionine. Cells were then labeled for 3 h with DMEM deficient in cysteine and methionine and containing Tran^{35}S-label (100 μCi/ml; MP Biomedicals). Following labeling, cells were washed 3 times with 3 ml of ice-cold PBS, and surface proteins were biotinylated using 1 mg/ml EZ-Link sulfo-NSH-biotin (Pierce) in PBS with rocking for 35 min at 4°C, followed by incubation at room temperature for 15 min. Cells were then washed 2 times with ice-cold PBS, lysed with 500 μl of RIPA lysis buffer, and processed as described above. Samples were analyzed using 10% SDS-PAGE and visualized using a Typhoon FLA 7000 imager (GE Healthcare Life Sciences).

Syncytium assay. Subconfluent Vero cells were transiently transfected with pCAGGS-Hendra F and pCAGGS-Hendra G at a ratio of 1:3 by use of Lipofectamine Plus reagent (Invitrogen) per the manufacturer's protocol. Syncytium formation was observed at 18 to 36 h posttransfection. Images were taken using a Nikon digital camera mounted atop a Nikon Eclipse TS100 microscope with a 10× objective.

Electron microscopy. HEK 293T (KY) cells were transfected to produce VLPs as described above. Five-microliter aliquots of concentrated VLPs were seeded on carbon-coated Formvar copper grids for 1 min. Grids were then washed once with double-distilled water for 1 min and incubated for 1 min with 5% uranyl acetate for negative staining. After complete drying of the samples, analysis was performed using a Philips BioTwin 12 transmission electron microscope.

Immunofluorescence microscopy. Vero cells seeded on poly-D-lysine-coated glass coverslips and grown to 50% confluence were transfected by use of Lipofectamine Plus reagents with plasmids pcDNA-Flag-HeV M (0.1 μg/well), pCAGGS-HeV F (0.2 μg/well), and/or pEGFP-C1-Rab11a (0.2 μg/well). At 24 h posttransfection, cells were washed three times with warm PBS for 10 min per wash, fixed with 4% paraformaldehyde in PBS for 15 min, and then washed three additional times. Cells were then permeabilized using 0.1% saponin, incubated in a blocking solution containing 1% bovine serum albumin (BSA) and 0.1% fish gelatin, and incubated with primary and secondary antibody solutions as described previously (55). For M/F colocalization studies, cells were bound with an F-specific antibody prior to fixation and permeabilization, to visualize only the cell surface-localized F protein, and incubated with an M-specific antibody after permeabilization. The HeV M protein was visualized using an anti-DDK monoclonal antibody specific to the Flag tag (Origene, Rockville, MD). The HeV F protein was visualized using mouse anti-HeV F MAb 7F7. Endogenous Rab11a was detected using a rabbit anti-Rab11a polyclonal antibody (Proteintech Group, Chicago, IL). The secondary antibodies used were Alexa Fluor 594-conjugated goat anti-mouse IgG2a for detection of M protein, Alexa Fluor 594-conjugated goat anti-mouse IgG1 for detection of F protein, and Alexa Fluor 488-conjugated goat anti-rabbit for detection of Rab11a. Washes were done after each antibody incubation, and cell nuclei were stained using ProLong Gold antifade reagent with DAPI (4′,6-diamidino-2-phenylindole) (Thermo Fisher Scientific). Cells were visualized with a Zeiss AxioImager M1 fluorescence microscope (Carl Zeiss Inc., Thornwood, NY), and images were captured using an Orca R2 digital camera (Hamamatsu Photonics, Bridgewater, NJ). Images were deconvolved using iVision software (BioVision Technologies, Exton, PA).

Statistical analysis. Analysis of the significance of differences for each corresponding group of experiments was done by the Student t test. Significance was set for P values of <0.05.

REFERENCES

1. Marsh GA, de Jong C, Barr JA, Tachedjian M, Smith C, Middleton D, Yu M, Todd S, Foord AJ, Haring V, Payne J, Robinson R, Broz I, Crameri G, Field HE, Wang LF. 2012. Cedar virus: a novel henipavirus isolated from Australian bats. PLoS Pathog 8:e1002836. https://doi.org/10.1371/journal.ppat.1002836.

2. Marsh GA, Wang LF. 2012. Hendra and Nipah viruses: why are they so deadly? Curr Opin Virol 2:242–247. https://doi.org/10.1016/j.coviro.2012.03.006.

3. Chua KB, Bellini WJ, Rota PA, Harcourt BH, Tamin A, Lam SK, Ksiazek TG, Rollin PE, Zaki SR, Shieh W, Goldsmith CS, Gubler DJ, Roehrig JT, Eaton B, Gould AR, Olson J, Field H, Daniels P, Ling AE, Peters CJ, Anderson LJ, Mahy BW. 2000. Nipah virus: a recently emergent deadly paramyxovirus. Science 288:1432–1435. https://doi.org/10.1126/science.288.5470.1432.

4. Halpin K, Young PL, Field HE, Mackenzie JS. 2000. Isolation of Hendra virus from pteropid bats: a natural reservoir of Hendra virus. J Gen Virol 81:1927–1932. https://doi.org/10.1099/0022-1317-81-8-1927.

5. Pernet O, Schneider BS, Beaty SM, LeBreton M, Yun TE, Park A, Zachariah TT, Bowden TA, Hitchens P, Ramirez CM, Daszak P, Mazet J, Freiberg AN, Wolfe ND, Lee B. 2014. Evidence for henipavirus spillover into human populations in Africa. Nat Commun 5:5342. https://doi.org/10.1038/ncomms6342.

6. Eaton BT, Broder CC, Middleton D, Wang LF. 2006. Hendra and Nipah viruses: different and dangerous. Nat Rev Microbiol 4:23–35. https://doi.org/10.1038/nrmicro1323.

7. Hyatt AD, Zaki SR, Goldsmith CS, Wise TG, Hengstberger SG. 2001. Ultrastructure of Hendra virus and Nipah virus within cultured cells and host animals. Microbes Infect 3:297–306. https://doi.org/10.1016/S1286-4579(01)01383-1.

8. Goldsmith CS, Whistler T, Rollin PE, Ksiazek TG, Rota PA, Bellini WJ, Daszak P, Wong KT, Shieh WJ, Zaki SR. 2003. Elucidation of Nipah virus morphogenesis and replication using ultrastructural and molecular approaches. Virus Res 92:89–98. https://doi.org/10.1016/S0168-1702(02)00323-4.

9. Halpin K, Bankamp B, Harcourt BH, Bellini WJ, Rota PA. 2004. Nipah virus conforms to the rule of six in a minigenome replication assay. J Gen Virol 85:701–707. https://doi.org/10.1099/vir.0.19685-0.

10. Schmitt PT, Ray G, Schmitt AP. 2010. The C-terminal end of parainfluenza virus 5 NP protein is important for virus-like particle production and

M-NP protein interaction. J Virol 84:12810–12823. https://doi.org/10.1128/JVI.01885-10.

11. Coronel EC, Takimoto T, Murti KG, Varich N, Portner A. 2001. Nucleocapsid incorporation into parainfluenza virus is regulated by specific interaction with matrix protein. J Virol 75:1117–1123. https://doi.org/10.1128/JVI.75.3.1117-1123.2001.

12. Takimoto T, Portner A. 2004. Molecular mechanism of paramyxovirus budding. Virus Res 106:133–145. https://doi.org/10.1016/j.virusres.2004.08.010.

13. Harrison MS, Sakaguchi T, Schmitt AP. 2010. Paramyxovirus assembly and budding: building particles that transmit infections. Int J Biochem Cell Biol 42:1416–1429. https://doi.org/10.1016/j.biocel.2010.04.005.

14. Pager CT, Dutch RE. 2005. Cathepsin L is involved in proteolytic processing of the Hendra virus fusion protein. J Virol 79:12714–12720. https://doi.org/10.1128/JVI.79.20.12714-12720.2005.

15. Pager CT, Craft WW, Jr, Patch J, Dutch RE. 2006. A mature and fusogenic form of the Nipah virus fusion protein requires proteolytic processing by cathepsin L. Virology 346:251–257. https://doi.org/10.1016/j.virol.2006.01.007.

16. Michalski WP, Crameri G, Wang L, Shiell BJ, Eaton B. 2000. The cleavage activation and sites of glycosylation in the fusion protein of Hendra virus. Virus Res 69:83–93. https://doi.org/10.1016/S0168-1702(00)00169-6.

17. Diederich S, Moll M, Klenk HD, Maisner A. 2005. The Nipah virus fusion protein is cleaved within the endosomal compartment. J Biol Chem 280:29899–29903. https://doi.org/10.1074/jbc.M504598200.

18. Popa A, Carter JR, Smith SE, Hellman L, Fried MG, Dutch RE. 2012. Residues in the Hendra virus fusion protein transmembrane domain are critical for endocytic recycling. J Virol 86:3014–3026. https://doi.org/10.1128/JVI.05826-11.

19. Diederich S, Sauerhering L, Weis M, Altmeppen H, Schaschke N, Reinheckel T, Erbar S, Maisner A. 2012. Activation of the Nipah virus fusion protein in MDCK cells is mediated by cathepsin B within the endosome-recycling compartment. J Virol 86:3736–3745. https://doi.org/10.1128/JVI.06628-11.

20. Meulendyke KA, Wurth MA, McCann RO, Dutch RE. 2005. Endocytosis plays a critical role in proteolytic processing of the Hendra virus fusion protein. J Virol 79:12643–12649. https://doi.org/10.1128/JVI.79.20.12643-12649.2005.

21. Weis M, Maisner A. 2015. Nipah virus fusion protein: importance of the cytoplasmic tail for endosomal trafficking and bioactivity. Eur J Cell Biol 94:316–322. https://doi.org/10.1016/j.ejcb.2015.05.005.

22. Vogt C, Eickmann M, Diederich S, Moll M, Maisner A. 2005. Endocytosis of the Nipah virus glycoproteins. J Virol 79:3865–3872. https://doi.org/10.1128/JVI.79.6.3865-3872.2005.

23. Whitman SD, Smith EC, Dutch RE. 2009. Differential rates of protein folding and cellular trafficking for the Hendra virus F and G proteins: implications for F-G complex formation. J Virol 83:8998–9001. https://doi.org/10.1128/JVI.00414-09.

24. Aguilar HC, Matreyek KA, Filone CM, Hashimi ST, Levroney EL, Negrete OA, Bertolotti-Ciarlet A, Choi DY, McHardy I, Fulcher JA, Su SV, Wolf MC, Kohatsu L, Baum LG, Lee B. 2006. N-glycans on Nipah virus fusion protein protect against neutralization but reduce membrane fusion and viral entry. J Virol 80:4878–4889. https://doi.org/10.1128/JVI.80.10.4878-4889.2006.

25. Wang YE, Park A, Lake M, Pentecost M, Torres B, Yun TE, Wolf MC, Holbrook MR, Freiberg AN, Lee B. 2010. Ubiquitin-regulated nuclear-cytoplasmic trafficking of the Nipah virus matrix protein is important for viral budding. PLoS Pathog 6:e1001186. https://doi.org/10.1371/journal.ppat.1001186.

26. Pentecost M, Vashisht AA, Lester T, Voros T, Beaty SM, Park A, Wang YE, Yun TE, Freiberg AN, Wohlschlegel JA, Lee B. 2015. Evidence for ubiquitin-regulated nuclear and subnuclear trafficking among Paramyxovirinae matrix proteins. PLoS Pathog 11:e1004739. https://doi.org/10.1371/journal.ppat.1004739.

27. Deffrasnes C, Marsh GA, Foo CH, Rootes CL, Gould CM, Grusovin J, Monaghan P, Lo MK, Tompkins SM, Adams TE, Lowenthal JW, Simpson KJ, Stewart CR, Bean AG, Wang LF. 2016. Genome-wide siRNA screening at biosafety level 4 reveals a crucial role for fibrillarin in henipavirus infection. PLoS Pathog 12:e1005478. https://doi.org/10.1371/journal.ppat.1005478.

28. Sun W, McCrory TS, Khaw WY, Petzing S, Myers T, Schmitt AP. 2014. Matrix proteins of Nipah and Hendra viruses interact with beta subunits of AP-3 complexes. J Virol 88:13099–13110. https://doi.org/10.1128/JVI.02103-14.

29. Amorim MJ, Bruce EA, Read EK, Foeglein A, Mahen R, Stuart AD, Digard P. 2011. A Rab11- and microtubule-dependent mechanism for cytoplasmic transport of influenza A virus viral RNA. J Virol 85:4143–4156. https://doi.org/10.1128/JVI.02606-10.

30. Bruce EA, Digard P, Stuart AD. 2010. The Rab11 pathway is required for influenza A virus budding and filament formation. J Virol 84:5848–5859. https://doi.org/10.1128/JVI.00307-10.

31. Chambers R, Takimoto T. 2010. Trafficking of Sendai virus nucleocapsids is mediated by intracellular vesicles. PLoS One 5:e10994. https://doi.org/10.1371/journal.pone.0010994.

32. Eisfeld AJ, Kawakami E, Watanabe T, Neumann G, Kawaoka Y. 2011. RAB11A is essential for transport of the influenza virus genome to the plasma membrane. J Virol 85:6117–6126. https://doi.org/10.1128/JVI.00378-11.

33. Katoh H, Nakatsu Y, Kubota T, Sakata M, Takeda M, Kidokoro M. 2015. Mumps virus is released from the apical surface of polarized epithelial cells, and the release is facilitated by a Rab11-mediated transport system. J Virol 89:12026–12034. https://doi.org/10.1128/JVI.02048-15.

34. Utley TJ, Ducharme NA, Varthakavi V, Shepherd BE, Santangelo PJ, Lindquist ME, Goldenring JR, Crowe JE, Jr. 2008. Respiratory syncytial virus uses a Vps4-independent budding mechanism controlled by Rab11-FIP2. Proc Natl Acad Sci U S A 105:10209–10214. https://doi.org/10.1073/pnas.0712144105.

35. Schmitt AP, Leser GP, Waning DL, Lamb RA. 2002. Requirements for budding of paramyxovirus simian virus 5 virus-like particles. J Virol 76:3952–3964. https://doi.org/10.1128/JVI.76.8.3952-3964.2002.

36. Li M, Schmitt PT, Li Z, McCrory TS, He B, Schmitt AP. 2009. Mumps virus matrix, fusion, and nucleocapsid proteins cooperate for efficient production of virus-like particles. J Virol 83:7261–7272. https://doi.org/10.1128/JVI.00421-09.

37. Ciancanelli MJ, Basler CF. 2006. Mutation of YMYL in the Nipah virus matrix protein abrogates budding and alters subcellular localization. J Virol 80:12070–12078. https://doi.org/10.1128/JVI.01743-06.

38. Patch JR, Crameri G, Wang LF, Eaton BT, Broder CC. 2007. Quantitative analysis of Nipah virus proteins released as virus-like particles reveals central role for the matrix protein. Virol J 4:1. https://doi.org/10.1186/1743-422X-4-1.

39. Kondo T, Yoshida T, Miura N, Nakanishi M. 1993. Temperature-sensitive phenotype of a mutant Sendai virus strain is caused by its insufficient accumulation of the M protein. J Biol Chem 268:21924–21930.

40. Yoshida T, Nagai Y, Maeno K, Iinuma M, Hamaguchi M, Matsumoto T, Nagayoshi S, Hoshino M. 1979. Studies on the role of M protein in virus assembly using a ts mutant of HVJ (Sendai virus). Virology 92:139–154. https://doi.org/10.1016/0042-6822(79)90220-4.

41. Runkler N, Pohl C, Schneider-Schaulies S, Klenk HD, Maisner A. 2007. Measles virus nucleocapsid transport to the plasma membrane requires stable expression and surface accumulation of the viral matrix protein. Cell Microbiol 9:1203–1214. https://doi.org/10.1111/j.1462-5822.2006.00860.x.

42. Mottet-Osman G, Iseni F, Pelet T, Wiznerowicz M, Garcin D, Roux L. 2007. Suppression of the Sendai virus M protein through a novel short interfering RNA approach inhibits viral particle production but does not affect viral RNA synthesis. J Virol 81:2861–2868. https://doi.org/10.1128/JVI.02291-06.

43. Gotoh B, Ohnishi Y, Inocencio NM, Esaki E, Nakayama K, Barr PJ, Thomas G, Nagai Y. 1992. Mammalian subtilisin-related proteinases in cleavage activation of the paramyxovirus fusion glycoprotein: superiority of furin/PACE to PC2 or PC1/PC3. J Virol 66:6391–6397.

44. Watanabe M, Hirano A, Stenglein S, Nelson J, Thomas G, Wong TC. 1995. Engineered serine protease inhibitor prevents furin-catalyzed activation of the fusion glycoprotein and production of infectious measles virus. J Virol 69:3206–3210.

45. Garten W, Hallenberger S, Ortmann D, Schafer W, Vey M, Angliker H, Shaw E, Klenk HD. 1994. Processing of viral glycoproteins by the subtilisin-like endoprotease furin and its inhibition by specific peptidyl-chloroalkylketones. Biochimie 76:217–225. https://doi.org/10.1016/0300-9084(94)90149-X.

46. Ortmann D, Ohuchi M, Angliker H, Shaw E, Garten W, Klenk HD. 1994. Proteolytic cleavage of wild type and mutants of the F protein of human parainfluenza virus type 3 by two subtilisin-like endoproteases, furin and Kex2. J Virol 68:2772–2776.

47. Mattera R, Farias GG, Mardones GA, Bonifacino JS. 2014. Co-assembly of viral envelope glycoproteins regulates their polarized sorting in neurons. PLoS Pathog 10:e1004107. https://doi.org/10.1371/journal.ppat.1004107.

48. Bhuin T, Roy JK. 2014. Rab proteins: the key regulators of intracellular

vesice transport. Exp Cell Res 328:1–19. https://doi.org/10.1016/j.yexcr .2014.07.027.

49. Nakatsu Y, Ma X, Seki F, Suzuki T, Iwasaki M, Yanagi Y, Komase K, Takeda M. 2013. Intracellular transport of the measles virus ribonucleoprotein complex is mediated by Rab11A-positive recycling endosomes and drives virus release from the apical membrane of polarized epithelial cells. J Virol 87:4683–4693. https://doi.org/10.1128/JVI.02189-12.

50. Brock SC, Goldenring JR, Crowe JE, Jr. 2003. Apical recycling systems regulate directional budding of respiratory syncytial virus from polarized epithelial cells. Proc Natl Acad Sci U S A 100:15143–15148. https://doi .org/10.1073/pnas.2434327100.

51. Rowe RK, Suszko JW, Pekosz A. 2008. Roles for the recycling endosome, Rab8, and Rab11 in hantavirus release from epithelial cells. Virology 382:239–249. https://doi.org/10.1016/j.virol.2008.09.021.

52. Dietzel E, Kolesnikova L, Sawatsky B, Heiner A, Weis M, Kobinger GP, Becker S, von Messling V, Maisner A. 2015. Nipah virus matrix protein influences fusogenicity and is essential for particle infectivity and stability. J Virol 90:2514–2522. https://doi.org/10.1128/JVI.02920-15.

53. Popa A, Pager CT, Dutch RE. 2011. C-terminal tyrosine residues modulate the fusion activity of the Hendra virus fusion protein. Biochemistry 50:945–952. https://doi.org/10.1021/bi101597k.

54. Pager CT, Wurth MA, Dutch RE. 2004. Subcellular localization and calcium and pH requirements for proteolytic processing of the Hendra virus fusion protein. J Virol 78:9154–9163. https://doi.org/10.1128/JVI.78.17 .9154-9163.2004.

55. Harrison MS, Schmitt PT, Pei Z, Schmitt AP. 2012. Role of ubiquitin in parainfluenza virus 5 particle formation. J Virol 86:3474–3485. https:// doi.org/10.1128/JVI.06021-11.